Sedimentary Geology 208 (2008) 27–35

Contents lists available at ScienceDirect

Sedimentary Geology

journal homepage: www.elsevier.com/locate/sedgeo

Phyllosilicate orientation demonstrates early timing of compactional stabilization in calcite-cemented concretions in the Barnett Shale (Late Mississippian), Fort Worth Basin, Texas (U.S.A)

Ruarri J. Day-Stirrat [a,*], Robert G. Loucks [a], Kitty L. Milliken [a,b], Stephen Hillier [c], Ben A. van der Pluijm [d]

[a] Bureau of Economic Geology, John A. and Katherine G. Jackson School of Geosciences, The University of Texas at Austin, University Station, Box X , Austin, TX, 78713, USA
[b] Department of Geological Sciences, John A. and Katherine G. Jackson School of Geosciences, The University of Texas at Austin, University Station, Box X , Austin, TX, 78713, USA
[c] Macaulay Institute, Craigiebuckler, Aberdeen, AB15 8QH, UK
[d] Department of Geological Sciences, University of Michigan, C.C. Little Building, 425 E. University Ave., Ann Arbor, MI 48109-1063, USA

ARTICLE INFO

Article history:
Received 21 December 2007
Received in revised form 8 April 2008
Accepted 16 April 2008

Keywords:
Barnett Shale
Goniometry
Concretions
Fabric

ABSTRACT

Calcite-cemented zones in the prolific gas-producing Barnett Shale (Ft. Worth Basin, Texas) preserve very early compactional fabrics that contrast markedly with fabrics in the enclosing host-rocks. The compactional state of these zones, based upon alignments of phyllosilicates as determined by High-resolution X-ray goniometry (HRXTG), complemented by X-ray powder diffraction (XRPD), back-scattered electron imaging, and elemental X-ray mapping, points to a prelithification, near-syndepositional timing of initial authigenic calcite emplacement. Thus, these carbonate-cemented zones are of particular interest for the information they provide on the character of grain assemblages and sediment types at the time of deposition and also on the early post-depositional environmental chemistry of the Barnett Shale strata.

1. Introduction

Deciphering the depositional environments represented by the diverse lithologies in the economically important Mississippian Barnett Shale is challenging because of a lack of modern analogues and extensive modification by diagenesis, especially compaction. Calcite-cemented lithologies in the Barnett Shale (*sensu stricto* concretions) are, potentially, of great interest because of the possibility that they preserve primary sediment characteristics that have been lost through compaction, dissolution, or replacement in the host-rocks (Woodland, 1984; Duck, 1990) and second, because they may provide information about the fluid chemistries at the sediment/water interface (Hudson, 1978; Coniglio and Cameron, 1990). Before utilizing calcite-cemented lithologies as a means to assess early sediment texture it is necessary to first convincingly document their early timing. This paper uses a combination of quantitative High-resolution X-ray goniometry (HRXTG), complemented by X-ray powder diffraction (XRPD), back-scattered electron (BSE) imaging, and X-ray elemental mapping to demonstrate that carbonate concretions in the Barnett Shale preserve early phyllosilicate compactional states that are consistent with the use of these lithologies as a 'window' into the character of sediments on the seafloor at the time of the Barnett Shale deposition.

1.1. Previous concretion studies

Nucleation and growth of concretions occur over a broad range of depths in the subsurface, from near the sediment water interface (e.g., Raiswell and Fisher, 2000 and discussions therein) to depths 3–4 km or more (e.g., Milliken et al., 1998). Internally, concretions typically manifest complex growth zonations that may arise from either a concentric or complex/pervasive growth mechanism (Mozley, 1996; Raiswell and Fisher, 2000; Hounslow, 2001; Mozley and Davis, 2005).

Early-formed calcite-cemented concretions in mudstone units may reveal the early post-depositional character of a sediment, as they may preserve original phyllosilicate textures (Oertel and Curtis, 1972; Woodland, 1984) and possibly clay flocs or aggregates (O'Brien, 1971), due to their uncompacted state relative to the encapsulating mudstone. Charting layer thicknesses as they increase towards the concretion is enough to demonstrate significant compaction in the host mudstone relative to the concretion. Pressure shadows adjacent to concretions (Lash and Blood, 2004b) also suggest early concretion solidification and later compaction of the host mudstone.

Historically, the mechanism that governs the reorientation of phyllosilicates into a preferred alignment has been attributed to mechanical processes, specifically, overburden-induced compaction (Sintubin, 1994; O'Brien, 1995). While this may adequately explain porosity reduction with increasing depth for fine-grained siliciclastic sediments (Athy, 1930; Hedberg, 1936; Dzevanshir et al., 1986; Dewhurst et al., 1998), it has been shown that mechanical compaction

* Corresponding author. Tel.: +1 512 471 7313; fax: +1 512 471 0140.
E-mail address: Ruarri.Day-Stirrat@beg.utexas.edu (R.J. Day-Stirrat).

0037-0738/$ – see front matter © 2008 Elsevier B.V. All rights reserved.
doi:10.1016/j.sedgeo.2008.04.007

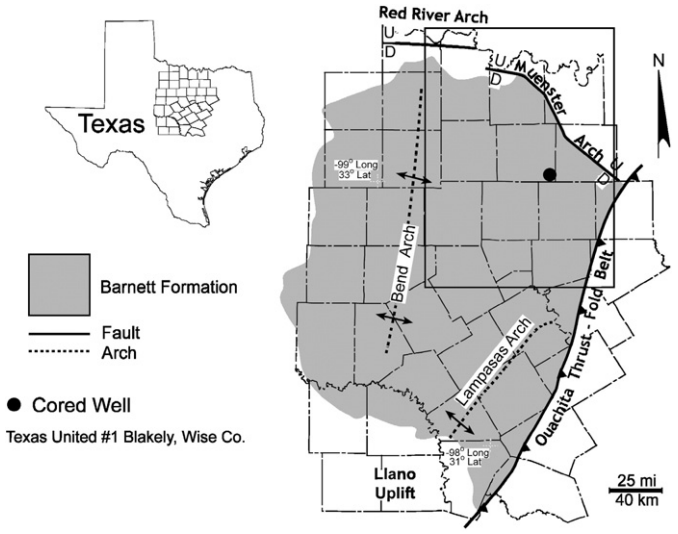

Fig. 1. Map of Barnett Shale extent and bounding geologic structures, with location of the Texas United #1 Blakely well (Modified from Loucks and Ruppel, 2007).

alone is not a significant driver of phyllosilicate reorientation (Matenaar, 2002; Charpentier et al., 2003; Worden et al., 2005; Aplin et al., 2006; Day-Stirrat et al., 2008). To achieve a preferred orientation, diagenetic phyllosilicates reactions, e.g., the smectite-to-illite transformation (Hower et al., 1976) may be critical (Ho et al., 1999; Charpentier et al., 2003; Worden et al., 2005; Day-Stirrat et al., 2008). These studies describe depositional phyllosilicate fabrics that have been preserved to considerable depths before diagenesis has imparted a preferred orientation.

2. Geologic setting, samples, and methods

The unconventional shale-gas system of the Mississippian Barnett Shale of the Fort Worth Basin (Fig. 1) is one of the most significant gas-producing reservoirs in Texas (Curtis, 2002; Montgomery et al., 2005; Pollastro et al., 2007). The U.S. Geological Survey estimates a mean volume of about 26 tcf of hydrocarbon gas in place. The Barnett Shale is marine in origin and comprises diverse lithologies, including laminated siliceous mudstones, laminated argillaceous lime mudstones, skeletal argillaceous lime packstones, (Loucks and Ruppel, 2007) and abundant carbonate concretions (Fig. 2). The Barnett Shale was deposited over 25 Ma (Osagean to Chesterian: 320–345 Ma) and unconformably overlies the karsted Ordovician Ellenburger Formation (McDonnell et al., 2007). The Fort Worth Basin is bounded to the east and southeast by the Ouachita structural front, to the south by the Llano Uplift, to the west by the Bend arch, and to the north and northeast by the Muenster and Red River arches. The formation thickness ranges from a few tens of meters along the western limit to more than 300 m adjacent to the Muenster arch (Pollastro et al., 2007). The core sample set from the Texas United #1 Blakely well is from a current burial depth of ~7200 ft (2188 m). The maximum burial is not well constrained as there may have been as much as 6000 ft (1824 m) of Pennsylvanian to late-Jurassic deposition and erosion (Ewing, 2006). Published gas maturity (equivalent vitrinite reflectance data, % Ro) places the Barnett Shale at 0.98–1.21% Ro (e.g. Hill et al., 2007; Pollastro et al., 2007) but there may have been areas of hydrothermal heating associated with regional faulting (Pollastro et al., 2007) that may have increased vitrinite reflectance values closer to 1.5% Ro. The present-day corrected bottom hole temperature for the Texas United #1 Blakely well is 200 °F (93 °C) at 7854 ft using the time-since-circulation method, but given the uncertainties surrounding the amount of Pennsylvanian to late-Jurassic deposition and erosion the maximum burial temperature is not well constrained. Equally, the timing of the fracturing and the mode of fracturing (Gale et al., 2007) is still under investigation but is undoubtedly related to the Pennsylvanian to late-Jurassic burial and erosion (Ewing, 2006). Petroleum production rates are dealt with fully by Pollastro et al. (2007) but it is pertinent to note that the average pore-throat radius is 50 Å (Bowker, 2007) making the Barnett Shale an extremely efficient seal in addition to being one of the most prolific gas reservoirs in Texas due to its high TOC (~4.0%) content (Jarvie et al., 2007).

In general, in outcrop carbonate-rich lithologies in the Barnett Shale clearly have the aspect of oblate and ellipsoidal concretions, ranging in size from a few centimetres up to half a meter in lateral extent (Fig. 2A, Papazis, 2005). The concretion margins are conformable with their enclosing mudstone host-rock. There are no signs of rotation of the lithified concretion as was also noted for the shale-hosted concretions described by Lash and Blood (2004a). In core (Fig. 2B) there is more ambiguity with respect to the nature of the calcite-cemented lithologies as the lateral continuity cannot be fully accessed. Nonetheless, the oblate shapes and lack of compaction are still, in many cases, apparent. There is no disruption of laminations or bedding by folding, implying that the maximum effective stress experienced by the Barnett Shale has always been in the vertical plane.

The Texas United #1 Blakely core has previously been described in terms of lithofacies and depositional setting (Loucks and Ruppel, 2007). Detailed core descriptions available in this previous paper were the basis for sample selection in this study. One sample from the Upper Barnett Shale was taken to represent host-rock 'black shale' in the Upper Barnett Shale (Sample B2, 7111 ft/2161.7 m) completely non-associated with calcite cementation. Sample B8 (7214 ft/2193.0 m) samples the host-rock 'black shale' lithology directly above a small cemented zone in the Lower Barnett Shale. Sample BH (7214 ft/2193.0 m) is just below sample B8 and spans from the upper boundary to the centre of the cemented zone. Sample B9 is taken from the centre of a cemented zone at 7218 ft (2194.3 m). Samples BJ and BI (7107 ft/2160.5 m) are additional samples that were used to make detailed petrographic examinations of the contacts between calcite-poor host-rock and calcite-rich lithologies.

2.1. X-ray power diffraction methodology

Mineralogical analyses by X-ray powder diffraction (XRPD) methods were made of the whole-rock bulk samples and of <2 sm clay-size fractions, obtained by gentle crushing, disaggregation,

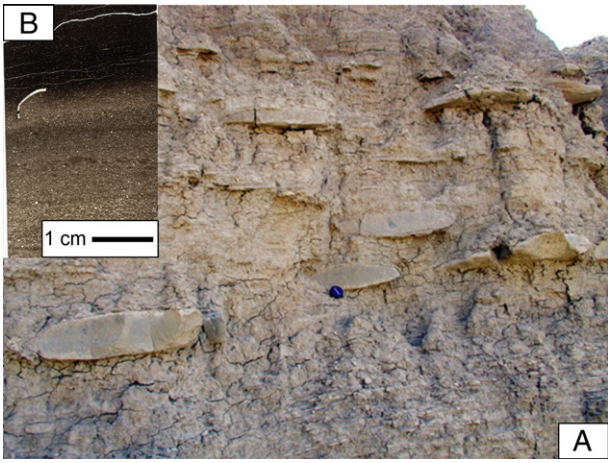

Fig. 2. A. Concretions in the outcrop of the Barnett Shale, San Saba County Texas. A lens cap is used for scale (From Loucks and Ruppel, 2007). B. A representative thin-section scan of a sample from the Texas United #1 Blakely well, Wise County, Texas (sample BI 7207 ft/2160.5 m) showing host-rock shale overlying a calcite-cemented lithology that in outcrop is interpreted to be a concretion.

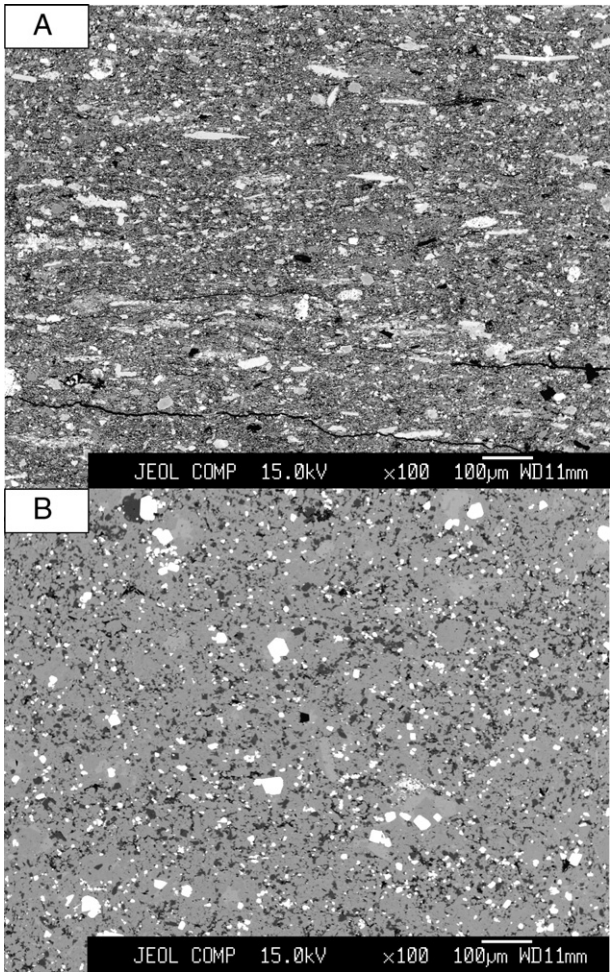

Fig. 3. A. BSE image of the host-rock sample B8 (7214 ft/2193.0 m) showing crude alignment of particles. B. The calcite-cemented lithology (sample B9, 7218 ft/2194.3 m). The calcite-cemented lithology no aligned fabric as compared to the host-rock.

dispersion and timed sedimentation. For whole-rock analysis the samples were prepared by McCrone milling of 3 g of sample in water, followed by spray drying of the resulting slurry to obtain random powder specimens, as described by Hillier (1999, 2002). Clay-size fractions were prepared by mounting the clay onto glass slides by a filter peel transfer method to obtain highly oriented specimens (Moore and Reynolds, 1997; Hillier, 2003). All XRPD patterns were recorded on a Siemens D5000 X-ray diffractometer, using Co-Kα radiation, selected by a diffracted beam graphite monochromator. Whole-rock samples were scanned from 2–75° 2Θ, counting for 2 s per 0.02° step. Clay-size fractions were scanned, from 2–45° 2Θ, counting for 1 s per 0.02° step, three separate scans were recorded: (1) in the air-dried state; (2) following glycolation by a vapour pressure method overnight; and (3) following heating to 350 °C for 1 h. Quantitative mineralogical determinations of whole-rock data are made by a full pattern fitting, normalized reference intensity ratio method, as described in Omotoso et al. (2006). Detailed identification of clay minerals in the clay-sized fraction was made by procedures given in Moore and Reynolds (1997) and Hillier (2003).

2.2. High-resolution X-ray texture methodology

Quantitative assessment of the alignment of phyllosilicates was made on an Enraf-Nonius CAD4 automated single-crystal diffractometer using the high resolution X-ray texture goniometry (HRXTG) method described by van der Pluijm et al. (1994). First, the samples were scanned over the range of 0.5–6.0° 2θ Mo (1–13° 2θ Cu). This indicated which clay mineral phases were present and determined the exact diffraction angles at which textural data were collected.

The second step of the measurement process involved the "pole-figure scan" (Ho et al., 1995), in which the degree of preferred orientation of previously identified phyllosilicates is determined. The goniometer and detector were fixed at the diffraction angle corresponding to the d-spacing of the 001 reflection of the chosen phase (identified in step one). Thin-sections of the sample, 200–500 μm thick cut perpendicular to bedding were rotated around two axes, one parallel to an imaginary line connecting the goniometer and detector (designated as φ), and one normal to it (designated as ω). Diffracted X-ray intensity data were collected every 2.5° between 0–360° around the φ axis, and in nine steps between 0–40° around the ω axis. In total, 1296 intensity measurements were made on each sample and corrected for sample absorption, grain density, and specimen thickness following van der Pluijm et al. (1994).

The degree of alignment is obtained from the intensity distribution of diffracted X-rays. Intensity data are displayed in pole-figure diagrams that show the distribution of crystallographic orientations in the form of poles to crystallographic planes. Pole-figure diagrams allow visualization of the spatial distribution of the X-ray intensities by displaying contour lines representing the pole distribution of phyllosilicate 001 plane orientations. More highly aligned fabrics yield

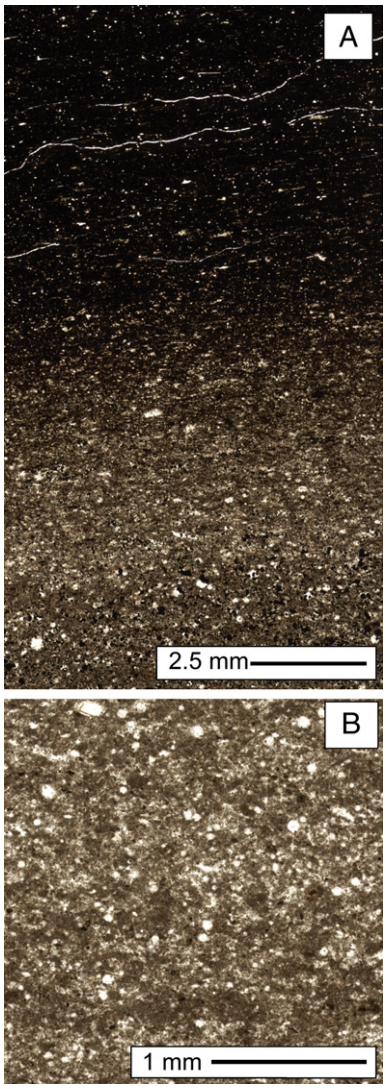

Fig. 4. A. The boundary between host-rock mudstone and calcite-cemented lithology below, Thin-section photograph is from sample Bi (7107 ft/2160.5 m). B. The uncompacted calcite-cemented lithology.

Table 1
Results (wt.%) of quantitative analysis of the whole-rock samples by the reference intensity ratios (RIR) method

Sample and depth	Sample ID	Quartz	Plagioclase	K-spar	Calcite	Dolomite/ ankerite	Siderite	Pyrite	Apatite	Muscovite mica 2M1	Illite–Smectite	Total clay
Blakely #1, 7111 ft/2161.7 m host-rock	B2	51.9	3.5	0.0	4.0	3.6	0.4	3.3	0.6	6.2	26.5	32.7
Blakely #1, 7214 ft/2193.0 m host-rock	B8	39.4	5.4	0.0	14.8	5.4	1.2	2.3	1.2	5.8	24.7	30.5
Blakely #1, 7214 ft/2193.0 m calcite-cemented lithology (Edge)	BH	11.6	2.0	0.0	72.5	3.0	0.3	4.0	0.8	0.0	5.8	5.8
Blakely #1, 7218 ft/2194.3 m calcite-cemented lithology (Centre)	B9	4.9	1.8	0.0	86.0	1.1	0.6	0.6	0.9	0.0	4.2	4.2

Table 2
Relative percentage of clay minerals in the <2 mm clay-size fraction and %expandability in illite-smectite

Sample and depth	Sample ID	Illite	Illite–smectite	%Exp
Blakely #1, 7111 ft/2161.7 m host-rock	B2	25	75	15
Blakely #1, 7214 ft/2193.0 m host-rock	B8	18	82	15
Blakely #1, 7214 ft/2193.0 m calcite-cemented lithology	BH	–	–	–
Blakely #1, 7218 ft/2194.3 m calcite-cemented lithology	B9	–	–	–

pole figures that can be contoured as concentric rings; completely random or isotropic fabrics (m.r.d. equal to 1.00) yield figures that have no poles. The degree of particle alignment is expressed as maximum pole density in multiples of a random distribution [m.r.d.] (Wenk, 1985), where higher values reflect higher degrees of alignment. Intensity is dependent on the concentration of crystals aligned parallel to each other. A value for the multiples of a random distribution is produced even when the sample has not been prepared perpendicular to bedding, so a stereographic projection showing centred contour lines validates the multiples of a random distribution value.

2.3. Potassium X-ray maps

Potassium was mapped by WDS (wave-length dispersive spectroscopy) under the following conditions: 15 KV accelerating voltage, sample current of 30 nA (measured on brass), and a focused electron beam (approximately 1 μm beam diameter). Mapping was performed on a 1024×1024 pixel grid, with 1 pixel equating to 1 μm; the dwell was 50 ms on each pixel. The X-ray maps are rendered as false colour images and consistent intensity levels were used on all images.

3. Results

Fig. 3 shows the general petrographic character of samples B8 (a host-rock) and B9 (a calcite-cemented lithology). The contrasting calcite content is apparent as are the gross differences in the degree of parallel orientation of the rock components.

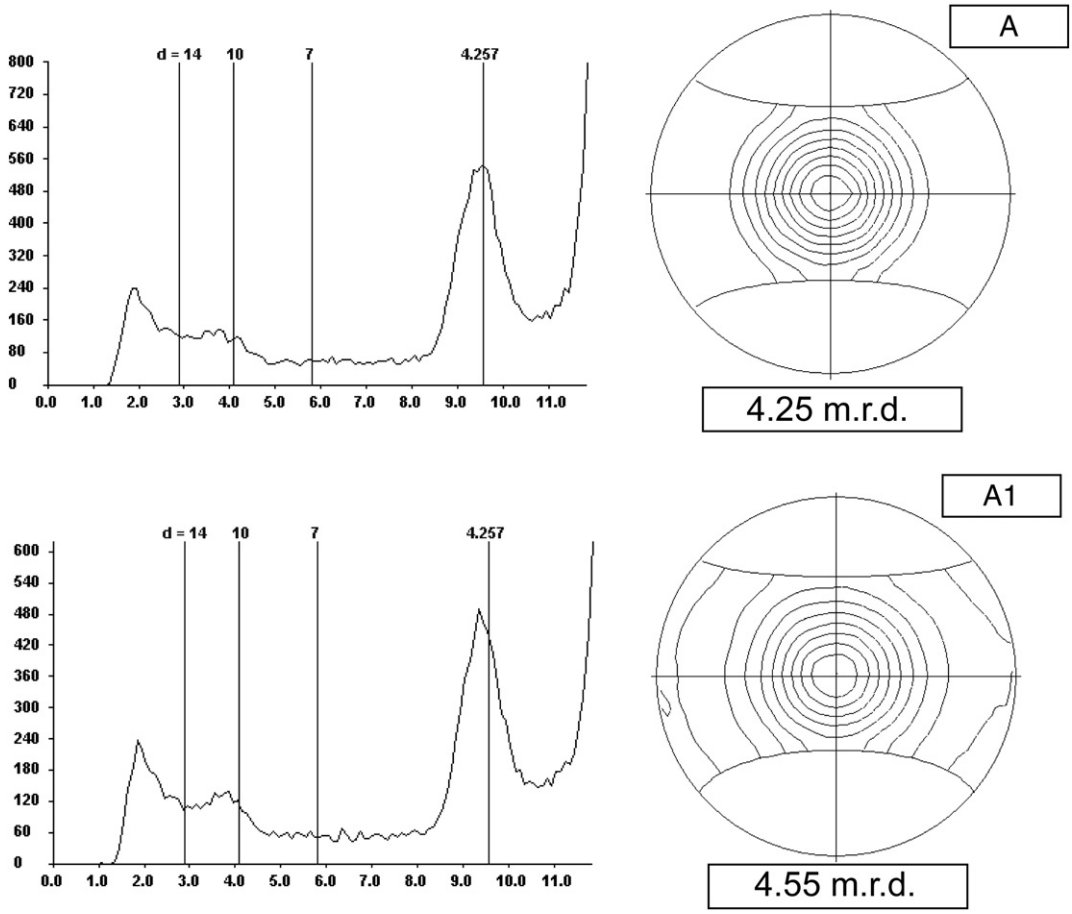

Fig. 5. Host-rock samples B2 (A) and B8 (A1), from 7111 ft (2161.7 m) and 7214 ft (2193.0 m) respectively. 2-Θ scans and the associated illite–smectite peak pole figures showing well centred contour lines and a moderately developed preferred orientation.

Textural and compositional heterogeneity also exists within the cemented lithologies (Fig. 4). At the transition between the host-rock and the cemented zone (Fig. 4A) the finely crystalline nature of the calcite component makes it very difficult to assess the degree to which the calcite is pore-filling. Nearer to the centre of the cemented zone (Fig. 4B), however, it is apparent that calcitic grains are present in addition to the likely cement. These grains have the form of micritic pellets, larger micritic intraclasts, and fossils including mollusks and spherical forms (possible calcispheres). These grains appear in far lesser amounts along the margins of the cemented zone and in the host-rock. Based on the abundance of these calcitic grains as seen in transmitted light images, it is clear that cement is not the only calcitic component within some of the cemented lithologies. Thus, the bulk calcite content cannot be used as a proxy for the porosity at the time of cementation and other methods must be used to estimate the degree of compaction.

3.1. Mineralogical analyses by X-ray power diffraction

Phyllosilicates in the clay-size fractions extracted from the two host-rock samples (B2, 7111 ft/2161.7 m and B8, 7214 ft/2193.0 m) consist of mixed-layer illite–smectite and discrete illite (Table 1). The illite–smectite has an expandability of around 15%, with peak positions consistent with R3 ordering (Table 2). In both samples the relative proportion of illite–smectite to illite is greater than 4:1. No other phyllosilicates are detectable but both clay-size fractions contain considerable amounts of quartz, suggesting that a large proportion of the quartz in the host-rock lithologies is of clay size. For the calcite-cemented lithologies (BH, 7214 ft/2193.0 m and B9, 7218 ft/2194.3 m), phyllosilicates were barely detectable in the clay-size fractions, both sets of XRPD patterns being dominated by calcite. Both host-rock samples show very similar compositions, consisting of quartz, plagioclase feldspar, calcite, dolomite, pyrite, apatite, 2M1 muscovite mica, mixed-layer illite–smectite, and a possible trace of siderite. The most obvious differences between the two host-rock samples are abundances of quartz and calcite. Peak positions of the calcite in the host-rock samples at approximately 3.030 Å indicate minor magnesium substitution.

Quartz contents (51.9–39.4%) of both host-rock samples are relatively high with respect to average mudstone (23.9% quartz Hillier, 2006 and references therein). Quartz peak widths at half peak height are also relatively wide 0.195° Δ2Θ (101 peak), compared to standard quartz (0.160 Δ2Θ) run under identical settings. This again indicates an important component of clay-size quartz in the host-rocks, which is probably diagenetic in origin. Macroscopically visible quartz replacement of mollusk shells is further confirmation that authigenic quartz precipitation has occurred in within the Barnett Shale (Papazis, 2005; Papazis and Milliken, 2005). Both calcite-cemented samples are composed mainly of calcite, but shifts in peak positions indicate that at least half of the calcite has significantly higher magnesium content compared to those in the host-rock. Thus sample BH at the calcite-cemented edge shows two calcite peak maxima at 3.030 and 3.015 Å, whilst the calcite from the centre of the calcite-cemented lithology in sample B9 presents a single broad, possibly composite peak, at around 3.022 Å. According to Milliman (1974) these values would indicate up to 10 mol% $MgCO_3$ substitution in some of the calcite.

Phyllosilicate contents of the host-rock shales are both around 25% mixed-layer illite–smectite, and around 6% 2M1 muscovite mica is also present. This compares with only 5% mixed-layer illite–smectite

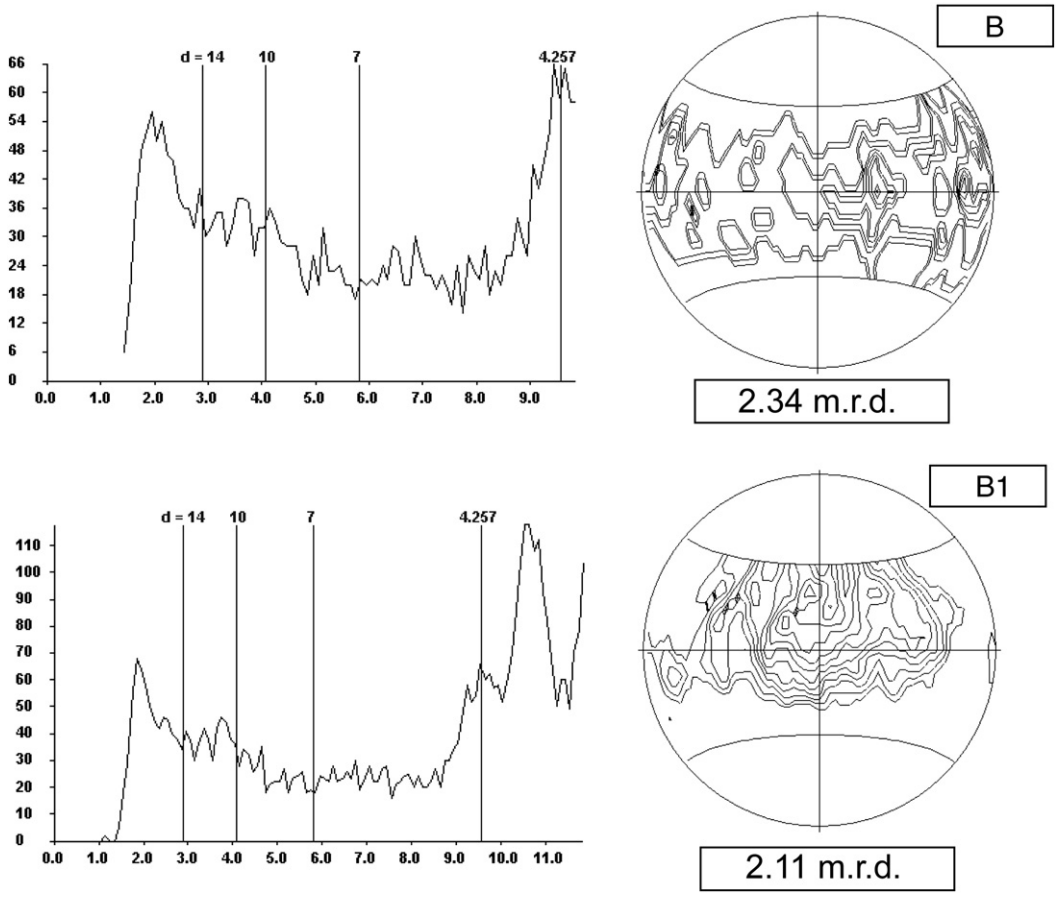

Fig. 6. Calcite-cemented lithology sample B9 (7218 ft/2194.3 m), 2-Θ scans and the associated illite–smectite peak pole figures showing poorly developed pole figures and a poorly developed preferred orientation, note the multiple poles.

in the calcite-cemented lithologies. Another feature of note is the fact that K-feldspar was not detected by XRPD. The limit of detection for K-feldspar is estimated at 0.5–0.7 wt.% at 95% confidence in the measured patterns (Hillier, 2003). Lastly, pyrite shows a trend of greatest abundance in the host-rock shale away from the calcite-cemented lithology and least abundance in the centre (Table 1).

3.2. Alignment of phyllosilicates by high-resolution X-ray texture goniometry

HRXTG data (Figs. 5 and 6) reveal strong quantifiable differences in the mixed-layer phase illite–smectite preferred alignment between calcite-cemented samples (sample B9, 7218 ft/2194.3), that has m.r.d. values of 2.34 and 2.11 (measurements taken at 3.76° 2-Θ and 3.78° 2-Θ, respectively), and host-rock samples (samples B2, 7111 ft/2161.7 m and B8, 7214 ft/2193.0 m), that were taken at 3.98° 2-Θ and 3.98° 2-Θ and have 4.25 and 4.55 m.r.d., respectively. The host-rock samples give a moderately strong alignment (Matenaar, 2002) and demonstrate little differences between the upper and lower Barnett Shale. The 2-Θ traces show a low abundance of 001 and 002 peaks of phyllosilicates relative to quartz, yet what illite–smectite material is present has a moderately strong alignment perpendicular to the maximum effective stress regime. The calcite-cemented lithology has even lower amounts of phyllosilicates as evidenced by the 2-Θ trace that barely stands above the background in the 001 and 002 phyllosilicate peak region. The illite–smectite material present has a poorly aligned fabric and a pole figure that has multiple poles and virtually no centre, this contrasts strongly with the host-rock samples. The calcite-cemented sample's X-ray intensity is barely above background consistent with the low concentration of phyllosilicates in this lithology relative to the host-rock (compare the XRPD data). However, the quantification of preferred orientation (m.r.d.) is independent of this X-ray intensity; it is a statistical test of the distribution of this intensity over the lower hemisphere equal area projection. The low m.r.d. values simply demonstrate that the measured phase has a low preferred orientation and is not a reflection of relative intensity.

3.3. Distribution of potassium

The potassium X-ray maps (Fig. 7) show the distribution of potassium-bearing phyllosilicate species in the host-rock (sample B2, 7111 ft/2161.7 m) and in the calcite-cemented lithology (sample B9, 7218 ft/2194.3). Potassium in K-feldspar is a very minor constituent of the Barnett Shale, one or two subhedral K-feldspars have been observed in the host-rock via BSE imaging and X-ray mapping (See Fig. 7A) and are below the lower limit of detection (0.5–0.7 wt.% (see Hillier, 2003)) in XRPD (Table 1) and are not observed in the calcite-cemented lithology. Isolated K-feldspar grains may be distinguished from potassium-bearing phyllosilicate species by their size, shape and the relative intensity of the X-ray elemental map. Fig. 7 shows one 10×10 μm potassium feldspar, with a red-pink 'colour intensity'. The other potassium-bearing species are interpreted to be potassium-bearing phyllosilicates, either illite, or high %I illite–smectite (XRPD has this percentage at ~85%I in the mixed-layer illite–smectite).

The bulk of the potassium in X-ray maps is distributed in the potassium-bearing phyllosilicates present, detrital micas, R1 or R3 illite–smectite. The host-rock has an apparent preferred orientation developed with some large (detrital) micas clearly distinguishing the preferred orientation. Finer grained I/S is also oriented perpendicular to maximum effective stress but its distribution is not necessarily homogeneous. Two distinct phyllosilicate drapes can be seen (Fig. 7A) with elevated levels of potassium-bearing phyllosilicates relative to the rest of the image area.

The calcite-cemented lithology, by contrast, has much lower concentrations of potassium-bearing phyllosilicates and the X-ray map (Fig. 7B) shows a random orientation of phyllosilicates and the appearance of a preserved 'cardhouse' structure (O'Brien, 1971). The phyllosilicate 'cardhouse' structure is filled with calcite cements that preserve this original fabric and clay mineral alignment.

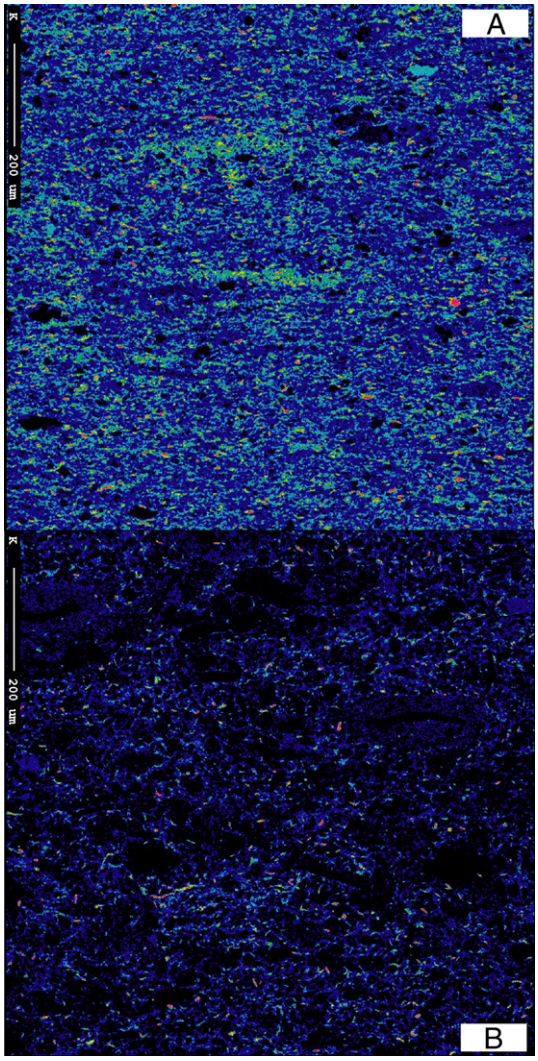

Fig. 7. A. Potassium X-ray map showing the R1 or R3 illite/smectite distribution in host-rock sample B2 (7111 ft/2161.7 m), some K is contained in isolated subhedral K-feldspar grains. B. Potassium X-ray map in the calcite-cemented lithology at 7218 ft/2194.3 m (sample B9).

4. Discussion

4.1. Phyllosilicate preferred orientation and initial concretion growth

The original work on phyllosilicate orientations in concretions by Oertel and Curtis (1972) demonstrated a preferred alignment decrease from the encapsulating host-rock contact to the concretion centre and implies a conventional concretion growth model (see Mozley, 1996; Raiswell and Fisher, 2000). The present study observes a similar effect in terms of the apparent lamination decrease towards the centre of the concretion (Figs. 2 and 4).

In the sample set described here the alignment quantification by HRXTG and the visualization of this alignment provided by the X-ray maps are consistent. An alignment in the host-rock of 4.25–4.55 m.r.d. points to significant realignment by mechanical and diagenetic processes. Comparable results in other basins (Fig. 8) suggest burial to greater than 100 °C or 3–4 km (Day-Stirrat et al., 2008), a range that is not outside of what is indicated by the observed degree of organic maturation in the Barnett Shale (Montgomery et al., 2005) and

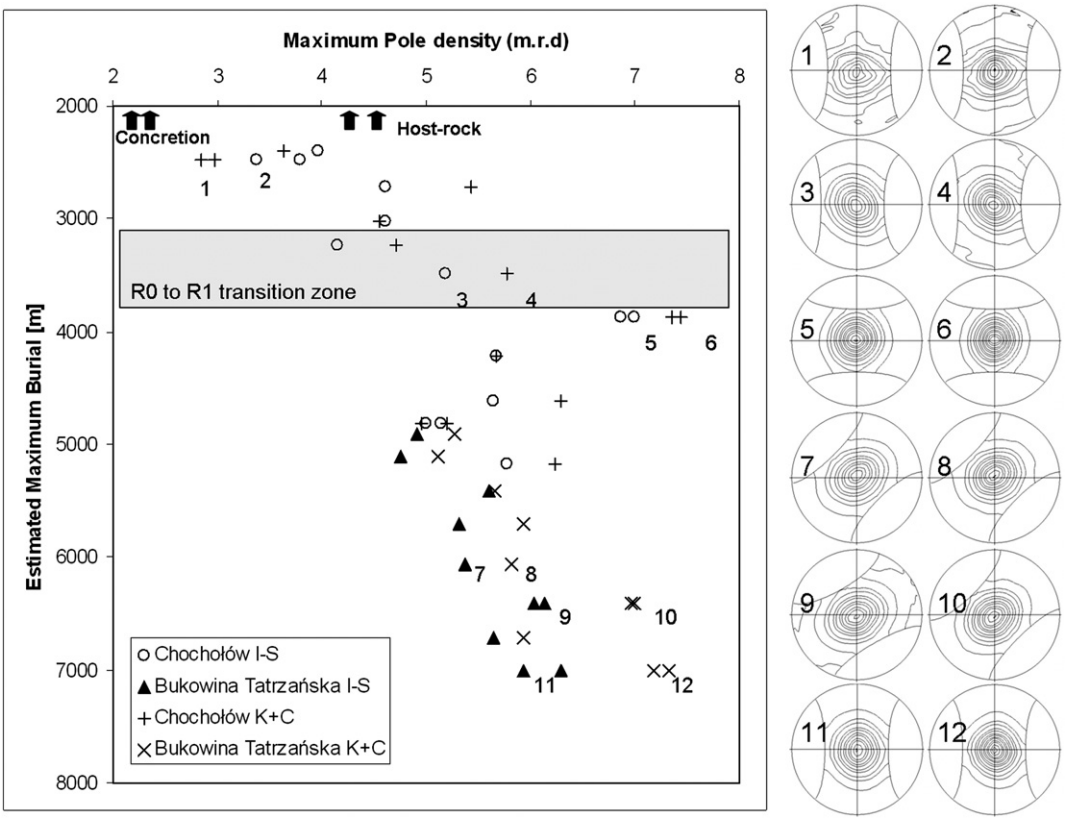

Fig. 8. A generalized plot of m.r.d. for samples from the Podhale Basin, Poland (Day-Stirrat et al., 2008), with estimated maximum burial. Compare to the values recorded for the Barnett Shale concretion and host-rock.

present-day burial depths and temperatures. The potassium X-ray maps provide visual confirmation of the high degree of phyllosilicate orientation in the host-rocks.

The orientation of the maximum effective stress in these rocks has been perpendicular to bedding. This assertion is based on three lines of evidence: (1) the orientation measurement by HRXTG is highest on a thin-section cut perpendicular to bedding; a cut normal to bedding has no preferred orientation (no basal phyllosilicate planes are normal to the X-ray beam in this situation); (2) the gross shape of the concretions is oblate with their long axis in the same orientation as bedding parallel fabric, indicating that no structural rotation has occurred; and (3) the fracture sets (Gale et al., 2007) are at a high angle (near vertical) which suggests that the greatest stress vector is in the vertical plane.

Considering compaction alone (without cementation), a host-rock porosity of less than 10% (greater than reality) and an average phyllosilicate content of ~25% (Table 1.), estimates by Yang and Aplin (2004) correspond to a maximum effective stress on the order of 25–30 MPa (greater in the case of lower porosity). However, it has been shown that mechanical rotation alone, in response to these high-effective stresses, is not to be the most significant driver of phyllosilicate reorientation (Ho et al., 1999; Matenaar, 2002; Charpentier et al., 2003; Worden et al., 2005; Day-Stirrat, 2006; Day-Stirrat et al., 2008), rather the effects of diagenesis are more significant with an R3 ordered type of illite–smectite indicative of and advanced degree of diagenesis. In other words the host-rock mudstones have a preferred phyllosilicate alignment that is governed by the vertical component of effective stress but is driven by phyllosilicate diagenesis.

The calcite-cemented samples display a significantly lower alignment of phyllosilicates (2.11 and 2.34 m.r.d.). A value of 1.00 m.r.d. is an isotropic fabric (Wenk, 1985) and almost never occurs even in unconsolidated sediment (Matenaar, 2002) because deposition always imparts some small degree of preferred alignment to phyllosilicates. Indeed, the lowest observed alignments in unconsolidated sediments are on the order of 1.70–1.90 m.r.d. (Matenaar, 2002), increasing to around 6.00 m.r.d. at the onset of metamorphism (Day-Stirrat et al., 2008) and ranging as high as 12.00 m.r.d. in metamorphic pelites (Jacob et al., 2000). There is no significant difference in the alignment values of the calcite-cemented lithology we record here and those of modern unconsolidated sediments. The value recorded here and the multi-poled pole figure (Fig. 6) strongly indicate very poor alignment.

The potassium X-ray map allows visualization of the above quantification, with 'cardhouse'-like and 'honeycomb'-like structures similar to those described and imaged by O'Brien (1971). Thus, the calcite-cemented lithology at 7218 ft (2194.3 m) appears to preserve an original depositional structure of flocculated phyllosilicate particles (Fig. 7B) similar to that described by O'Brien (1971) and Bennett et al. (1991). In order to resist the effects of mechanical compaction and later diagenetic change, an early-formed cement must have supported the voids in this very open stacking structure.

The higher amounts of calcite observed in the concretion centres as compared to their more outer zones suggest that the degree of cement emplacement may not have been uniform across cemented bodies. The complication, of course, is that the primary content of calcitic particulate debris may also have varied across the layers encompassed by the concretion.

The presence of magnesium calcite points to a marine depositional environment and the preservation of this marine phase by early cementation. Although, it is clear that very early compactional states are preserved, this does not preclude the possibility that some portion of the calcite formed later and at greater burial depths (e.g. Raiswell and Fisher, 2000) as only small amounts of cement (Klein et al., 1999; Raiswell and Fisher, 2000) may lead to substantial increases in the

strength of muddy sediment (e.g. Karig, 1996). Pervasive early cement may serve to lock the phyllosilicate preferred orientation to a near-random orientation rather than cementing the whole concretion. It is clear that this precursor lithification was strong enough to resist early burial compaction and was also able to prevent compactional crushing of cephalopod fossils (see Figure 14 in Loucks and Ruppel, 2007).

The full determination of the entirety of the calcite genesis is not necessary in order to assess the compactional state as revealed by the phyllosilicate component. The results from HRXTG and X-ray mapping indicate that the concretions of the Barnett Shale are, indeed, of great relevance for investigations into the primary character of the sediments. The host-rock mudstone may be more phyllosilicate-rich than the concretion because concretion growth was nucleated in a particular volume and phyllosilicate concentrations were simply diluted. An alternative interpretation, with more dramatic mass balance implications, is that the original host-rock may have been more calcite-rich in terms of having calcite detritus matching that observed in the concretions, but altered through diagenesis and fluid flow to leave a siliciclastic-dominated composition.

5. Conclusions

1. Calcite-rich lithologies in the Barnett shale contain both authigenic and detrital carbonates.
2. HRXRG indicates that compaction, and perhaps chemical diagenesis as well, has served to impart a high degree of phyllosilicate alignment in calcite-poor Barnett lithologies ("black shale").
3. HRXRG demonstrates that calcite-cemented lithologies in the Barnett preserve a very early phyllosilicate compactional state.
4. X-ray mapping of potassium allows visual confirmation of the relative alignment of K-rich phyllosilicates.
5. Primary sediment characteristics preserved by early cementation make the calcite-cemented lithologies of the Barnett Shale of great interest for deciphering the depositional conditions of this economically important unit.

Acknowledgments

The STARR program at the Bureau of Economic Geology supplied funding for the project. The HRXTG facility is supported by NSF grant 047707 (van der Pluijm) and the EMAL at the university of Michigan. We thank Richard Worden and an anonymous reviewer for their thorough and thought-provoking reviews.

References

Aplin, A.C., Matenaar, I.F., McCarty, D.K., van der Pluijm, B.A., 2006. Influence of mechanical compaction and clay mineral diagenesis on the microfabric and pore-scale properties of deep-water Gulf of Mexico mudstones. Clays and Clay Minerals 54 (4), 500–514.

Athy, A.F., 1930. Density, porosity and compaction of sedimentary rocks. AAPG Bulletin 14, 1–24.

Bennett, R.H., O'Brien, N.R., Hulbert, H., 1991. Determinants of clay and shale microfabric signatures: processes and mechanisms. In: Bennett, R.H., Bryant, W.R., Hulbert, M.H. (Eds.), Microstructure of Fine-Grained Sediments. Springer Verlag.

Bowker, K.A., 2007. Barnett Shale gas production, Fort Worth Basin: issues and discussion. AAPG Bulletin 91 (4), 523–533.

Charpentier, D., Worden, R.H., Dillon, C.G., Aplin, A.C., 2003. Fabric development and the smectite to illite transition in Gulf of Mexico mudstones: an image analysis approach. Journal of Geochemical Exploration 78–79, 459–463.

Coniglio, M., Cameron, J.S., 1990. Early diagenesis in a potential oil-shale — evidence from calcite concretions in the Upper Devonian Kettle Point Formation, south-western Ontario. Bulletin of Canadian Petroleum Geology 38 (1), 64–77.

Curtis, J.B., 2002. Fractured shale-gas systems. AAPG Bulletin 86, 1921–1938.

Day-Stirrat, R.J., 2006. Diagenetic controls on the phyllosilicate fabric of mudstones. Ph. D. Thesis, University of Newcastle-Upon-Tyne, Newcastle-Upon-Tyne, UK, 375 pp.

Day-Stirrat, R.J., Aplin, A.C., Srodon, J., van der Pluijm, B.A., 2008. Diagenetic reorientation of phyllosilicate minerals in Palaeogene mudstones of the Podhale Basin, southern Poland. Clays and Clay Minerals 56 (1), 98–109.

Dewhurst, D.N., Aplin, A.C., Sarda, J.P., Yang, Y.L., 1998. Compaction-driven evolution of porosity and permeability in natural mudstones: an experimental study. Journal of Geophysical Research-Solid Earth 103 (B1), 651–661.

Duck, R.W., 1990. SEM study of clastic fabrics preserved in calcareous concretions from the Late-Devensian Errol Beds, Tayside. Scottish Journal of Geology 26, 33–39.

Dzevanshir, R.D., Buryakovskiy, L.A., Chilingarian, G.V., 1986. Simple quantitative-evaluation of porosity of argillaceous sediments at various depths of burial. Sedimentary Geology 46 (3–4), 169–175.

Ewing, T.E., 2006. Mississippian Barnett Shale, Fort Worth basin, north-central Texas: gas-shale play with multi-trillion cubic foot potential: discussion. AAPG Bulletin 90 (6), 963–966.

Gale, J.F.W., Reed, R.M., Holder, J., 2007. Natural fractures in the Barnett Shale and their importance for hydraulic fracture treatments. AAPG Bulletin 91 (4), 603–622.

Hedberg, H.D., 1936. Gravitational compaction of clays and shales. American Journal of Sciences 31, 241–287.

Hillier, S., 1999. Use of an air brush to spray dry samples for X-ray powder diffraction. Clay Minerals 34 (1), 127–135.

Hillier, S., 2002. Spray drying for X-ray powder diffraction preparation. IUCR Commission on Powder Diffraction Newsletter 27 (27), 7–9.

Hillier, S., 2003. Quantitative analysis of clay and other minerals in sandstones by X-ray powder diffraction (XRPD). In: Worden, R.H., Morad, S. (Eds.), International Association of Sedimentologists Special Publication 34: Clays and Clay Cements in Sandstones. Blackwell, Oxford, pp. 213–251.

Hillier, S., 2006. Chapter 3. Formation and alteration of clay materials. In: Reeves, G.M., Sims, I., Cripps, J.C. (Eds.), Clay Materials used in Construction, Geological Society, London, Engineering Geology Special Publications, pp. 29–71.

Hill, R.J., Jarvie, D.M., Zumberge, J., Henry, M., Pollastro, R.M., 2007. Oil and gas geochemistry and petroleum systems of the Fort Worth Basin. AAPG Bulletin 91 (4), 445–473.

Ho, N.C., Peacor, D.R., van der Pluijm, B.A., 1995. Reorientation mechanisms of phyllosilicates in the mudstone-to-slate transition at Lehigh Gap, Pennsylvania. Journal of Structural Geology 17 (3), 345–356.

Ho, N.C., Peacor, D.R., van der Pluijm, B.A., 1999. Preferred orientation of phyllosilicates in Gulf Coast mudstones and relation to the smectite-illite transition. Clays and Clay Minerals 47 (4), 495–504.

Hounslow, M.W., 2001. The crystallographic fabric and texture of siderite in concretions: implications for siderite nucleation and growth processes. Sedimentology 48 (3), 533–557.

Hower, J., Eslinger, E.V., Hower, M.E., Perry, E.A., 1976. Mechanism of burial metamorphism of argillaceous sediment 1. Mineralogical and chemical evidence. Geological Society of America Bulletin 87 (5), 725–737.

Hudson, J.D., 1978. Concretions, isotopes, and diagenetic history of Oxford Clay (Jurassic) of central England. Sedimentology 25 (3), 339–369.

Jacob, G., Kisch, H.J., van der Pluijm, B.A., 2000. The relationship of phyllosilicate orientation, X-ray diffraction intensity ratios, and c/b fissility ratios in metasedimentary rocks of the Helvetic zone of the Swiss Alps and the Caledonides of Jamtland, central western Sweden. Journal of Structural Geology 22 (2), 245–258.

Jarvie, D.M., Hill, R.J., Ruble, T.E., Pollastro, R.M., 2007. Unconventional shale-gas systems: the Mississippian Barnett Shale of north-central Texas as one model for thermogenic shale-gas assessment. AAPG Bulletin 91 (4), 475–499.

Karig, D.E., 1996. Uniaxial reconsolidation tests on porous sediments; mudstones from Site 897, Texas A&M University, Ocean Drilling Program, College Station, TX, United States.

Klein, J.S., Mozley, P., Campbell, A., Cole, R., 1999. Spatial distribution of carbon and oxygen isotopes in laterally extensive carbonate-cemented layers: implications for mode of growth and subsurface identification. Journal of Sedimentary Research 69 (1), 184–201.

Lash, G.G., Blood, D., 2004a. Geochemical and textural evidence for early (shallow) diagenetic growth of stratigraphically confined carbonate concretions, Upper Devonian Rhinestreet black shale, western New York. Chemical Geology 206 (3–4), 407–424.

Lash, G.G., Blood, D.R., 2004b. Origin of shale fabric by mechanical compaction of flocculated clay: evidence from the Upper Devonian Rhinestreet Shale, western New York, USA. Journal of Sedimentary Research 74 (1), 110–116.

Loucks, R.G., Ruppel, S.C., 2007. Mississippian Barnett Shale: lithofacies and depositional setting of a deep-water shale-gas succession in the Fort Worth Basin, Texas. AAPG Bulletin 91 (4), 579–601.

Matenaar, I.F., 2002. Compaction and microfabric rearrangement of fine-grained siliciclastic sediments. Ph. D. Thesis, University of Newcastle-Upon-Tyne, Newcastle-Upon-Tyne, UK, 253 pp.

McDonnell, A., Loucks, R.G., Dooley, T., 2007. Quantifying the origin and geometry of circular sag structures in northern Fort Worth Basin, Texas: paleocave collapse, pull-apart fault systems, or hydrothermal alteration? AAPG Bulletin 91 (9), 1295–1318.

Milliken, K.L., et al., 1998. Geochemical history of calcite precipitation in Tertiary sandstones, Northern Apennines, Italy. In: Morad, S. (Ed.), Carbonate Cementation in Sandstones. IAS Special, vol. 26, pp. 213–240.

Milliman, J.D., 1974. Marine carbonates — part 1. In: Milliman, J.D., Muller, G., Forstner, U. (Eds.), Recent sedimentary carbonates. Springer Verlag, New York.

Montgomery, S.L., Jarvie, D.M., Bowker, K.A., Pollastro, R.M., 2005. Mississippian Barnett Shale, Fort Worth basin, north-central Texas: gas-shale play with multi-trillion cubic foot potential. AAPG Bulletin 89 (2), 155–175.

Moore, D.M., Reynolds, R.C.J., 1997. X-ray diffraction and the identification and analysis of clay minerals. Oxford University Press, Oxford, New York.

Mozley, P.S., 1996. The internal structure of carbonate concretions in mudrocks: a critical evaluation of the conventional concentric model of concretion growth. Sedimentary Geology 103 (1–2), 85–91.

Mozley, P.S., Davis, J.M., 2005. Internal structure and mode of growth of elongate calcite concretions: evidence for small-scale, microbially induced, chemical heterogeneity in groundwater. Geological Society of America Bulletin 117 (11–12), 1400–1412.

O'Brien, N.R., 1971. Fabric of kaolinite and illite floccules. Clays and Clay Minerals 19, 353–359.
O'Brien, N.R., 1995. Origin of shale fabric-clues from framoids. Northeastern Geology and Environmental Sciences 17, 146–150.
Oertel, G., Curtis, C.D., 1972. Clay-ironstone concretion preserving fabrics due to progressive compaction. Geological Society of America Bulletin 83 (9), 2597–2605.
Omotoso, O., McCarty, D.K., Hillier, S., Kleeberg, R., 2006. Some successful approaches to quantitative mineral analysis as revealed by the 3rd Reynolds Cup contest. Clays and Clay Minerals 54 (6), 748–760.
Papazis, P.K., 2005. Petrographic characterization of the Barnett Shale, Fort Worth Basin, Texas. Master of Science Thesis, The University of Texas at Austin, Austin, 142 pp.
Papazis, P. K., Milliken, K. L., 2005. Cathodoluminescent Textures and the origin of quartz in the Mississippian Barnett Shale, Fort Worth Basin, Texas: American Association of Petroleum Geologists Annual Meeting (Calgary, Canada), Abstracts volume, p. A105.
Pollastro, R.M., Jarvie, D.M., Hill, R.J., Adams, C.W., 2007. Geologic framework of the Mississippian Barnett Shale, Barnett-Paleozoic total petroleum system, Bend arch-Fort Worth Basin, Texas. AAPG Bulletin 91 (4), 405–436.
Raiswell, R., Fisher, Q.J., 2000. Mudrock-hosted carbonate concretions: a review of growth mechanisms and their influence on chemical and isotopic composition. Journal of the Geological Society 157, 239–251.
Sintubin, M., 1994. Clay fabrics in relation to the burial history of shales. Sedimentology 41, 1161–1169.
van der Pluijm, B.A., Ho, N.-C., Peacor, D.R., 1994. High-resolution X-ray texture goniometry. Journal of Structural Geology 16, 1029–1032.
Wenk, H.-R., 1985. Measurement of pole figures. In: Wenk, H.-R. (Ed.), Preferred Orientation in Deformed Metals and Rocks; An Introduction to Modern Texture Analysis. Acad. Press, Orlando, FL, pp. 11–47.
Woodland, B.G., 1984. Fabric of the clastic component of Carboniferous concretions and their enclosing matrix. In: Belt, B.S., MacQueen, R.W. (Eds.), Neuvieme Congres International de Stratigrahie et de Geologie du Carbonifere, 3: Washington and Champaign-Urbana. Southern Illinois University Press, Carbondale and Edwardsville, Illinois.
Worden, R.H., Charpentier, D., Fisher, Q.J., Aplin, A.C., 2005. Fabric development and the smectite to illite transition in Upper Cretaceous mudstones from the North Sea: an image analysis approach. In: Shaw, R.P. (Ed.), Understanding the Micro to Macro Behaviour of Rock-Fluid Systems. Geological Society, London, pp. 103–114. Special Publications.
Yang, Y.L., Aplin, A.C., 2004. Definition and practical application of mudstone porosity-effective stress relationships. Petroleum Geoscience 10 (2), 153–162.